# Lattice-dynamics study of $Cs_2SiF_6$ with application to the vibronic optical spectra of $MnF_6^{-2}$ in $Cs_2SiF_6$

H. H. Patterson*
*Department of Chemistry, University of Maine, Orono, Maine 04473*

J. W. Lynn†
*Department of Physics, Brookhaven National Laboratory, Upton, New York 11973*
(Received 28 July 1978)

Neutron scattering, Raman, and infrared absorption measurements have been made to study the lattice dynamics of cesium hexafluorosilicate (IV), a cubic antifluorite-type material. Dispersion relations for normal modes of vibration, with energies less than 20 meV (160 $cm^{-1}$), along the [ξ00], [ξξξ], and [ξξ0] symmetry directions have been determined by coherent-inelastic-neutron-scattering experiments. Light scattering measurements were used to determine the Raman-active zone-center vibrations, while infrared spectra showed both fundamental and combination bands. The rigid-ion lattice-dynamics model of O'Leary and Wheeler was fit to the available experimental data, and gave a reasonably good representation of the lattice dynamics. The model was then used to calculate the phonon density of states for $Cs_2SiF_6$. Phonon structure present in the luminescence spectra of $MnF_6^{-2}$ in $Cs_2SiF_6$ has been compared with the $Cs_2SiF_6$ phonon-density-of-states calculation. Selection rules have been used to assign the low-energy vibronic structure to high-symmetry critical points in the Brillouin zone of $Cs_2SiF_6$.

## I. INTRODUCTION

Materials of the form $Cs_2MF_6$ (e.g., $M$ = Ge, Si) have the cubic antifluorite crystal structure in which the $M$ ions occupy a face-centered cubic lattice and possess cubic point symmetry. The $M$-type ions can be substitutionally replaced by many types of impurity ions and, because of the high symmetry of the impurity sites, these materials are good candidates for optical studies of the electronic spectra of the impurity ions. Generally, the electronic and lattice-dynamical properties are strongly interrelated, and it then becomes highly desirable to have a thorough understanding of the lattice dynamics of the host material. We have therefore undertaken a study of the vibrational spectra of $Cs_2SiF_6$ using neutron, infrared, and light scattering techniques.

In recent years a large number of high-resolution $MX_6^{-2}$ octahedral impurity ion optical studies at liquid-helium temperature have been reported,[1] and the experimental spectra are characterized by detailed phonon structure. In an attempt to understand these data, comparisons have been made with Raman and infrared determined zone-center vibrational energies, where a high density of phonon states is likely to occur. However, these are not the only phonons that participate in the electronic transition and, in fact, there are generally more experimental vibronic peaks than expected from such a simple isolated-ion model. Also, an isolated-ion model is inadequate to understand recent Zeeman polarization studies.[2]

In an attempt to describe the lattice dynamics of $A_2MX_6$ antifluorite-type systems, O'Leary and Wheeler[3] (OLW) have carried out a series of crystallographic and spectroscopic experiments on $K_2ReCl_6$, a substance which exhibits four phase transitions below room temperature. They were able from symmetry considerations to assign a number of phonons to zone-center and zone-boundary phonons, and to use a rigid-ion lattice-dynamics model to predict phonon dispersion curves. Durocher and Dorain,[4] using the (OLW) model, calculated the phonon density of states of $K_2ReCl_6$ and compared these results with the detailed 4 K optical-absorption spectra for impurities of $Os^{+4}$ and $Re^{+4}$ in single crystals of $K_2PtCl_6$. Their analysis provided strong evidence that the previously used isolated-ion model was inadequate. Further, they pointed out that vibrations that have even inversion symmetry at the zone center may become odd at other positions in the Brillouin zone, and thus can be very important in assigning phonon structure present in optical transitions.

Recently, Chodos and Satten[5] have proposed a lattice-dynamical model for $Cs_2UBr_6$ to assign the vibronic sidebands in this antifluorite cubic material. Their seven-parameter model employed a Urey-Bradley valence force field for the short-range interactions and standard long-range Coulomb terms. Only zone-center infrared and Raman data were used to determine numerical values of the seven force constants. Nevertheless, this calculation showed the importance of considering the entire Brillouin zone in assigning the optical spectra of impurity ions in crystals.

 

Finally, Chodos, Black, and Flint[6] have recently reported a lattice-dynamics analysis of the $^2E_g \rightarrow {}^4A_{2g}$ detailed luminescence spectra for $Cs_2MnF_6$ and $A_2MF_6$:$MnF_6^{-2}$ mixed crystal systems with the $A_2MF_6$ host lattice having $M$ = Si, Ge, and $A$ = K, Rb. The experimental optical spectra were compared with the calculated phonon dispersion curves for $Cs_2MnF_6$ to assign the low-energy lattice vibronic structure.

With the recent use of various lattice-dynamical models to interpret the detailed optical spectra of $MX_6^{-2}$ complexes, it is important to test these models for their reliability. Inelastic neutron measurements are the best approach because phonon energies versus wave-vector dispersion relations can be obtained directly from experiment. Once a proper foundation of the lattice dynamics and its influence on the optical spectra of ions in these crystals has been established, optical measurements in new systems can then be used to obtain the energies and symmetries of lattice vibrations not available from Raman and infrared measurements. Thus we have studied $K_2ReCl_6$ and $Cs_2SiF_6$ by inelastic neutron scattering. $Cs_2SiF_6$ is known to have the same face-centered cubic structure between 4–300 K while $K_2ReCl_6$ has displacive phase transitions which occur by a soft rotary mechanism. The $K_2ReCl_6$ study is reported elsewhere.[7] Here we will confine our attention to $Cs_2SiF_6$.

The organization of this paper is as follows. In Sec. II the optical experimental details will be reported, and in Sec. III the phonon dispersion measurements will be discussed. In Sec. IV the lattice-dynamics analysis will be presented, and in Sec. V the optical data will be assigned from the lattice-dynamical model results.

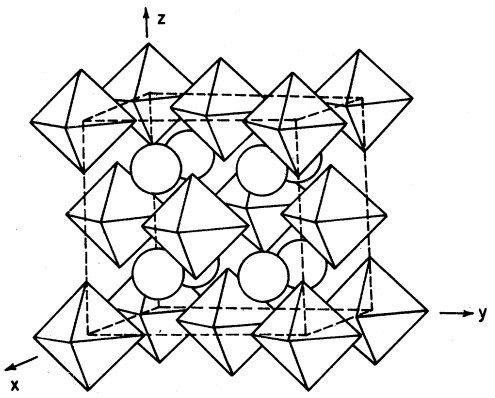


FIG. 1. Schematic representation of the $Cs_2SiF_6$ antifluorite lattice. The circles depict the $Cs^+$ ions. The octahedra represent the $SiF_6^{-2}$ ions and occupy a face-centered cubic lattice with Si ions residing in the center of each octahedra and the six F ions at the corners.

## II. OPTICAL MEASUREMENTS

### A. Crystal details

$Cs_2SiF_6$ possesses the antifluorite crystal structure with space group $O_h^5(Fm3m)$. The structure is the same as that of $CaF_2$, with the replacement of $Ca^{+2}$ by an $SiF_6^{-2}$ octahedral complex ion, and the $F^-$ ion by a $Cs^+$ cation. The $SiF_6^{-2}$ ions form a face-centered cubic lattice as shown in Fig. 1, with $F$ atoms located along the six equivalent cubic axes a distance $u$ (unspecified by symmetry) from the silicon atom.

The primitive unit cell contains nine atoms, and thus there are 27 phonon branches in the vibrational spectrum. In Table I the symmetries and

TABLE I. Summary of zone-center vibrational modes.

| Irreducible representation | Description | Activity | Energy, $cm^{-1}$ |
|---|---|---|---|
| $\Gamma^{1+}$ ($\nu_1$) | Symmetric internal mode | Raman | 647 [a] |
| $\Gamma^{3+}$ ($\nu_2$) | Stretching internal mode | Raman | 469 [a] |
| $\Gamma^{4-}$ ($\nu_3$) | Stretching internal mode | Infrared | 740 [c] |
| $\Gamma^{4-}$ ($\nu_4$) | Bending internal mode | Infrared | 470 [c] |
| $\Gamma^{5+}$ ($\nu_5$) | Bending internal mode | Raman | 401 [a] |
| $\Gamma^{5-}$ ($\nu_6$) | Bending internal mode | Inactive | d |
| $\Gamma^{4-}$ | Optical mode | Infrared | 96–106 for TO |
| $\Gamma^{4+}$ | Rotary mode | Inactive | 88 [b] |
| $\Gamma^{4-}$ | Acoustic mode | ... | 0 |
| $\Gamma^{5+}$ | $Cs^+$ motion | Raman | 68.8 [a] |

[a] Raman measurements carried out at liquid-helium temperatures.
[b] Determined from inelastic neutron measurements at 6 K.
[c] Infrared measurements carried out at liquid-nitrogen temperature.
[d] Determined from infrared combination band analysis to be about 265 $cm^{-1}$ at the zone center.

activities of the zone-center vibrational modes are given. Fifteen branches correspond to internal mode vibrations of the $SiF_6^{-2}$ octahedral complex. These vibrational energies are greater than 200 $cm^{-1}$, or 25 MeV (1 MeV = 8.066 $cm^{-1}$), and no attempt has been made to study them by neutron scattering. The remaining vibrational modes are of four types: acoustic, $Cs^+$-ion motion, octahedral rotary motion, and optical mode motion with the cations and anions moving out of phase. The rotary mode is neither Raman or infrared active at the zone center. This mode has been of much interest in $K_2ReCl_6$[3,7] and is responsible for at least two displacive phase transitions in this material.

The $Cs_2SiF_6$ single crystals were grown from a 40% hydrofluoric acid solution by slow evaporation over a period of about a month. The dimensions of the largest single crystal was about $2 \times 6 \times 6$ mm and the crystal was colorless. The unit-cell length of this cubic crystal was determined from elastic neutron scattering experiments to be 8.92 Å at room temperature and 8.82 Å at 5 K.

### B. Raman measurements

Raman experiments were carried out on a single $Cs_2SiF_6$ crystal at 6 K to determine the Raman-active zone-center mode energies. A krypton laser with excitation at 530.9 and 520.8 nm was used. The scattered radiation was detected by means of a photon counting setup which has been described previously.[8]

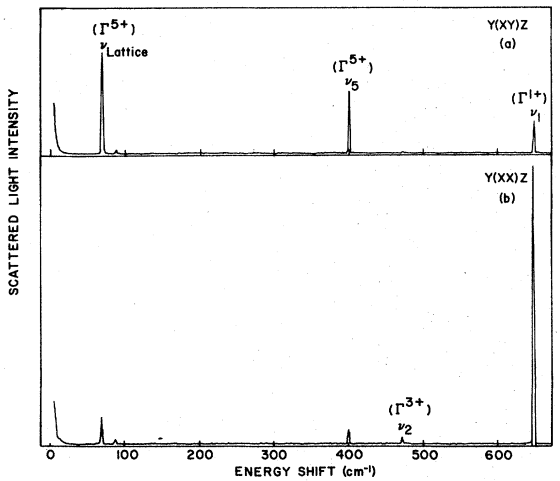


FIG. 2. Raman spectrum at liquid-helium temperature for $Cs_2SiF_6$ single crystal with laser excitation at 5309 Å showing the dependence of the scattered light intensity on the Raman polarizability tensor component. In (a) and (b), with 90° scattering, the $\alpha_{xy}$ and $\alpha_{xx}$ Raman tensor components, respectively, are shown. The intensity of scattering is proportional to $|\alpha_{ab}|^2$.

The Raman spectrum for $Cs_2SiF_6$ at 6 K is displayed in Fig. 2. From polarization considerations the peak at 647 $cm^{-1}$ can be assigned to the symmetric stretch mode $\nu_1$. Also, the 469- and 401-$cm^{-1}$ peaks can be assigned to the $\nu_2$ asymmetric stretch and $\nu_5$ bending modes, respectively. The 68.8 $cm^{-1}$ peak must be assigned to the $\Gamma^{5+}$ zone-center cation motion lattice mode. These assignments are in agreement with literature results for $Cs_2SiF_6$.[9]

### C. Infrared measurements

Infrared absorption experiments between 250 and 1500 $cm^{-1}$ were carried out for $Cs_2SiF_6$, at room temperature and liquid-nitrogen temperature, to observe possible combination and overtone peaks. A Beckman infrared spectrophotometer was used. A $Cs_2SiF_6$ powder sample was pressed into a pure clear pellet about 0.1 mm thick. The experimental data are shown in Fig. 3 and the IR energies are listed in Table II. From the relative intensities of the various peaks, it is reasonable to assign the 474- and 722-$cm^{-1}$ peaks as due to the $\nu_4$ bending and $\nu_3$ stretching modes, respectively. The remaining peaks are due to combination excitations and their assignments will be discussed in Sec. V.

## III. INELASTIC NEUTRON MEASUREMENTS

The inelastic neutron scattering measurements were done on triple-axis spectrometers at the High Flux Beam Reactor at Brookhaven. The monochromator was a (002) curved pyrolytic graphite crystal and the analyzer was a (002) pyrolytic flat graphite crystal. For the inelastic measurements 20′ or 40′ full width at half maximum (FWHM) Söller slits were placed both before and after the monochromator and the analyzer to limit the horizontal divergence of the neutron beam. Most of the measurements were performed with the scattered neutron energy fixed at 24.0 MeV and the incident neutron energy variable between 24 and 43 MeV, so that the cross section for the creation of phonons was measured.[10] The constant $\vec{Q}$ mode of operation was used always, where

$$\vec{Q} = \vec{K}_i - \vec{K}_f = \vec{\tau} + \vec{q} \tag{1}$$

Here, $\vec{K}_i$ and $\vec{K}_f$ are the initial and final wave vectors of the neutron, $\hbar\vec{Q}$ is the momentum transferred to the crystal, $\vec{\tau}$ is a reciprocal lattice vector, and $\vec{q}$ is the wave vector of the phonon.

From coherent inelastic scattering experiments one can determine the frequencies, wave vectors, and polarizations of the normal modes of vibra-

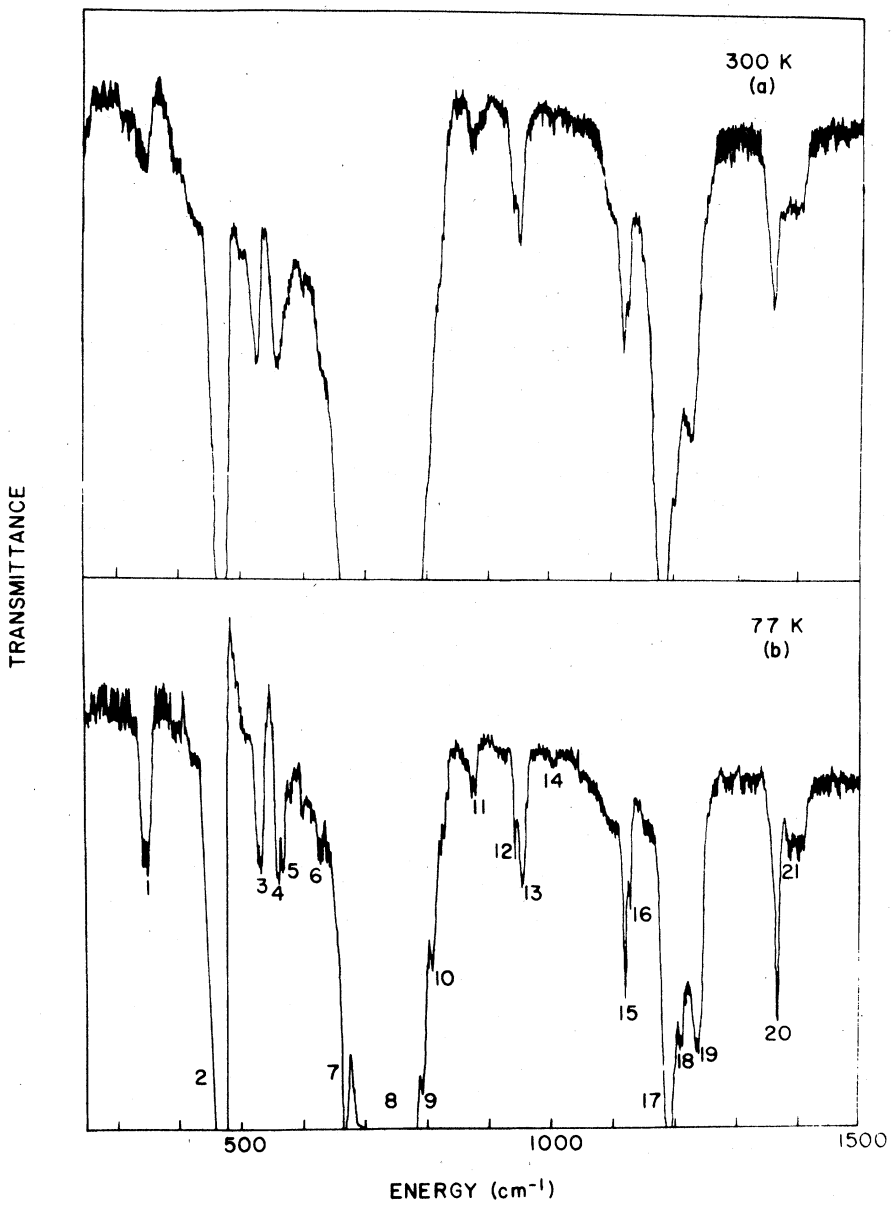


FIG. 3. Infrared spectrum of a pure pressed $Cs_2SiF_6$ pellet at (a) room and (b) liquid-nitrogen temperatures. Peaks 2 and 8 are assigned to the $\nu_4(\Gamma^{4-})$ and $\nu_3(\Gamma^{4-})$ fundamental internal modes. The strong peak 17 is assigned to a $\nu_2+\nu_3$ combination band. In Table II our assignments for all of the peaks are tabulated.

tions of a single crystal. It can be shown that the differential cross section for coherent inelastic scattering is given by[10]

$$\sigma_j(K_i \to K_f) = \frac{\hbar}{2}\frac{K_f}{K_i}\begin{pmatrix} N_j \\ N_j+1 \end{pmatrix} g_j^2(\vec{q},\vec{\tau}) \qquad (2)$$

for a constant $\vec{Q}$ scan. With phonon annihilation, the thermal population factor $N_j = [\exp(h\nu/KT)-1]^{-1}$ is used, and for phonon creation, $N_j+1$ is used. The $e^{-2W}$ factor is the Debye-Waller factor. The quantity

$$g_j^2(\vec{q},\vec{\tau}) = \sum_k \left| \frac{b_k \vec{Q}\cdot\vec{\xi}_{jk}(\vec{q})}{[M_k \nu_j(\vec{q})]^{1/2}} \times \exp(i\vec{Q}\cdot\vec{R}_k)\exp(-W(Q)) \right|^2 \qquad (3)$$

is the dynamical structure factor, with $R_k$ the position of the $k$th atom in the unit cell, and $b_k$ its coherent-neutron-scattering amplitude. Also, $\xi_{jk}(\vec{q})$ is the polarization vector of the $k$th atom with mass $M_k$. Expression (2) indicates that the intensity of inelastic scattering for a one-phonon process is directly proportional to the inelastic structure factor $g_j^2(\vec{q},\vec{\tau})$; thus from a lattice-dy-

TABLE II. Assignments for $Cs_2SiF_6$ infrared spectrum.

| Peak no. | Energy, $cm^{-1}$ (77 K) | Assignment | Remarks |
|---|---|---|---|
| 1 | 350 | $\nu_6{}^a(240) + LO^a(110) = 350$ | Becomes sharper at 77 K |
| 2 | 470 | $\nu_4$ | |
| 3 | 533 | $\nu_4(470) + \Gamma^{5+}(69) = 539$ | |
| 4 | 560 | $\nu_4(470) + \Gamma^{4+}(88) = 558$ | |
| 5 | 568 | $\nu_2(469) + TO(100) = 569$ | Appears at 77 K |
| 6 | 638 | $\nu_5{}^a(401) + \nu_6{}^a(240) = 641$ | Appears sharp at 77 K |
| 7 | 668 | $\nu_5(401) + \nu_6(265) = 666$ | Appears sharp at 77 K |
| 8 | 740 | $\nu_3$ | |
| 9 | 795 | $3\nu_6(265) = 795$ | Shoulder |
| 10 | 800 | $\nu_3(740) + \Gamma^{5+}(68) = 808$ | Shoulder; appears at 77 K |
| 11 | 874 | $\nu_4(470) + \nu_5(401) = 871$ | |
| 12 | 945 | $\nu_2(469) + \nu_4(474) = 943$ | |
| 13 | 958 | | |
| 14 | 1005 | | |
| 15 | 1120 | $\nu_1(647) + \nu_4(470) = 1117$<br>$\nu_3(722) + \nu_5(401) = 1121$ | Becomes sharp at 77 K |
| 16 | 1130 | | |
| 17 | 1192 | $\nu_2(469) + \nu_3(722) = 1191$ | |
| 18 | 1212 | $\nu_2(469) + \nu_3(741) = 1210$ | |
| 19 | 1240 | | Appears sharper at 77 K |
| 20 | 1370 | $\nu_1(647) + \nu_3(722) = 1369$ | Appears sharper at 77 K |
| 21 | 1390 | $2\nu_1(647) + TO(96) = 1390$ | Appears sharper at 77 K |

[a]The lattice-dynamical calculations indicate these energies at the $L$ symmetry point.

namical model one should be able to predict suitable reciprocal lattice vectors $\vec{\tau}$ at which to observe the energy of the $j$th vibrational branch at a given wave vector $\vec{q}$.

Initially, to observe the transverse and longitudinal acoustic modes, $g_j^2(\vec{q}, \vec{\tau})$ was calculated for about 100 different reciprocal lattice vectors. The eigenvectors used were from the O'Leary and Wheeler rigid-ion lattice-dynamical model[3] (to be discussed in Sec. IV) with the same force constants as reported by OLW for $K_2ReCl_6$ but with the masses, positions of atoms, and scattering amplitudes appropriate for $Cs_2SiF_6$. Using the predictions of this calculation for suitable $\tau$ vectors at which to observe the acoustic modes in the $[\xi 00]$, $[\xi\xi\xi]$, and $[\xi\xi 0]$ reciprocal-lattice directions, inelastic neutron scattering experiments were carried out.

From the acoustic-mode neutron results and available Raman and infrared data for $Cs_2SiF_6$, the 14 parameters of the OLW dynamical model were refined. The new eigenfunctions were then used to predict suitable reciprocal lattice vectors at which to observe the rotary, and optical transverse and longitudinal modes. The transverse and longitudinal optical-mode branches, as well as the degenerate rotary mode component, were observed in the $\Delta$, $\Lambda$, and $\Sigma$ reciprocal space high-symmetry directions (see Fig. 4) at room temperature. In the experimental $(hkk)$ scattering plane the nondegenerate rotary mode has a small value of $g_j^2$ and we did not observe this mode.[7]

Finally, the inelastic structure factor calculations predicted that away from the zone center, for many reciprocal-lattice vectors, the transverse optical (TO) and degenerate rotary mode components have about the same energies and structure factors. Thus we had to look for selected reciprocal positions to distinguish between the rotary and TO modes. Also, the structure factor calculations indicated small values of $g_j^2$ for the optical mode which involves mostly the $Cs^+$-ion motion. Fortunately, Raman measurements at liquid-helium temperature were able to determine

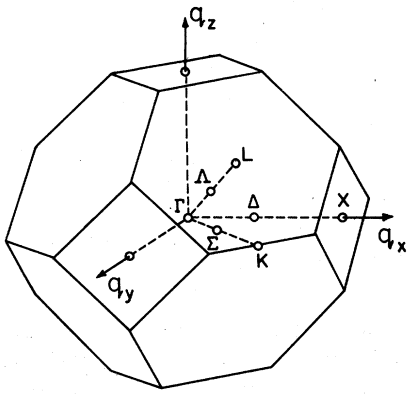


FIG. 4. Face-centered cubic Brillouin zone appropriate for $Cs_2SiF_6$.

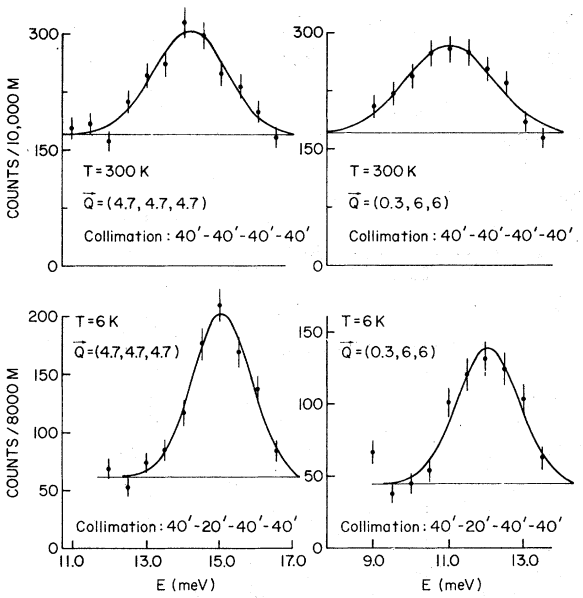


FIG. 5. Sample inelastic neutron scattering data for the transverse and longitudinal optic phonons at 300 and 6 K. Note that the signal-to-noise ratio improves at lower temperatures, in contrast to the usual situation for phonon scattering. The solid curves represent a least-squares fit of a Gaussian function to the data.

the zone-center energy to be 68.8 $cm^{-1}$ or 8.53 MeV.

If the inelastic neutron scattering measurements at room temperature are compared with the 6-K results, it is found that the phonon energies generally shift uniformly to higher energies by 6% as the temperature is lowered. This increase in the average phonon energy is expected since the lattice constant decreases by about 1%. We also remark that there was a substantial improvement at low temperatures in the signal-to-noise for many of the higher-energy phonons. Figure 5 shows sample experimental data for transverse and longitudinal optical phonons at room temperature and 6 K. Usually the signal-to-noise ratio decreases at low temperatures due to the decrease in the phonon thermal population factor $N_j$. However, a decrease in $N_j$ can sometimes be compensated by an increase in the Debye-Waller factor $e^{-2W}$. Moreover, there is a substantial change in the "background" with temperature, which is due to a decrease of the multiphonon scattering. These higher-order phonon cross sections generally vary relatively slowly as a function of wave vector and energy, and therefore appear as background.

## IV. LATTICE DYNAMICAL MODEL

The lattice-dynamical model that we used for $Cs_2SiF_6$ is a 14-parameter rigid-ion model developed by O'Leary and Wheeler.[3] It does not take account of the polarizabilities of the ions. The model was originally developed to describe the dispersion relations in $K_2ReCl_6$ in the high-symmetry cubic phase and to provide a basis for understanding the structural phase transitions that occur in this material. One complication with the lattice-dynamics analysis is that the Si–F separation is not determined by symmetry; thus, the force constants must be consistent with the observed atom-atom equilibrium separation.

The OLW model considers the atoms to interact with central forces that can be separated into a short-range part that acts between neighboring atoms only and a long-range electrostatic interaction between the ionic charges. Ten parameters describe the short-range interaction of the Si-F(2), Cs-F(2), Cs-Cs(2), and F-F(4) atoms about a single octahedron. Four parameters describe the interactions between the F atoms on neighboring octahedra. The long-range Coulomb interactions are described by effective charges for the Cs, Si, and F atoms. Electrical neutrality reduces the number of independent charge-type parameters to 2. Also, the stability conditions that (i) the Si–F distance must be the equilibrium value and (ii) the crystal must be in a state of vanishing stress means that the total number of independent parameters is reduced to 14.

The experimental inelastic neutron scattering results along the $\Delta$, $\Lambda$, and $\Sigma$ symmetry directions, as well as the Raman and infrared zone-center data, were fit to the OLW rigid-ion model by use of the CDC 7600 computer at Brookhaven. Initially, the internal vibrational mode zone-center energies were least-squares fit by variation only of the six force constant parameters that involve Si-F and F-F atomic motions. Then, the lattice-mode data with energies less than 200 $cm^{-1}$ were least-squares fit by variation of the remaining eight force constant parameters that involve Cs-Cs, F-F neighboring octahedra interactions, as well as the effective charges of the atoms. In the final least-squares fit, both the internal vibrational mode $\Gamma$ data and the lattice-mode dispersion data were fit by variation of all the fourteen force constant parameters. The final dispersion results for the OLW model are shown in Fig. 6 by the solid lines. The force constants are given in Table III. A detailed discussion of this lattice-dynamical model and the definitions of the force constants can be found in Ref. 3.

The least-squares fit of the (Fig. 6) experimental data to the OLW model gives an rms deviation of .27 MeV (2.2 $cm^{-1}$). The good fit demonstrates that the OLW rigid-ion model is capable of a reasonable description of the lattice dynamics for

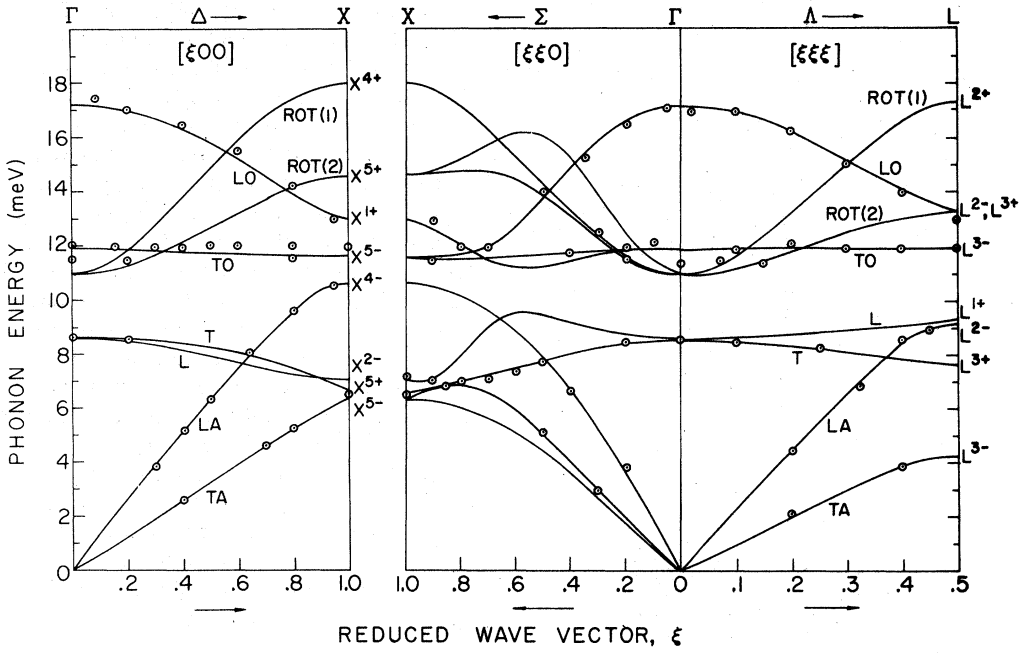


FIG. 6. Phonon dispersion results for $Cs_2SiF_6$ at 6 K in the Δ, Λ, and Σ directions. Experimental data represented by circles. The solid lines correspond to dispersion curves calculated from the O'Leary and Wheeler rigid-ion model with the lattice-dynamics parameters of Table III.

a system such as $Cs_2SiF_6$ in which the ligand is a small atom with a small polarizability.

### A Phonon frequency distribution function

The calculation of the phonon density of states was carried out by the extrapolation procedure of Gilat and Raubenheimer.[11] The method involves dividing the irreducible 1/48th portion of the Brillouin zone into a mesh of equally spaced points. The secular dynamical equation

$$|D_{ij}(\vec{q}) - \omega^2\delta_{ij}| = 0 \quad (i,j = 1,27) \tag{4}$$

is diagonalized at each equally spaced point in reciprocal space and other solutions between the spaced points are found by linear interpolation. If the mesh is sufficiently fine, this procedure will lead to an accurate density of states. However, for a complicated lattice-dynamical problem such as the cubic antifluorite $Cs_2SiF_6$ case, the dynamical matrix that must be diagonalized at each mesh point is $27 \times 27$. The diagonalization of such a large matrix requires a considerable amount of computer time; thus the ultimate accuracy of $g(\omega)$ will be limited by available computer

TABLE III. Lattice-dynamics parameters.[a]

| Parameter | Value | |
|---|---|---|
| Atom | Charge | |
| Si | 1.19 | |
| F | −0.52 | |
| Cs | 0.97 | |
| Force constant | Parallel | Perpendicular |
| F3(0,0,0)–F4(0,0,0) | 0.56 (mdyn/Å) | −0.14 (mdyn/Å) |
| F3(0,0,0)–F4($\frac{1}{2}$,−$\frac{1}{2}$,0) | 0.013 | 0.032 |
| F2(0,0,0)–F4(0,0,0) | 0.22 | 0.017 |
| F2(0,0,0)–F4($\frac{1}{2}$,−$\frac{1}{2}$,0) | −0.002 | −0.037 |
| F3(0,0,0)–Cs8(0,0,0) | 0.11 | −0.012 |
| Cs8(0,0,0)–Cs9(0,0,0) | 0.0009 | 0.003 |
| Si(0,0,0)–F4(0,0,0) | 2.33 | 0.45 |

[a]The parameters are each defined in Ref. 3.

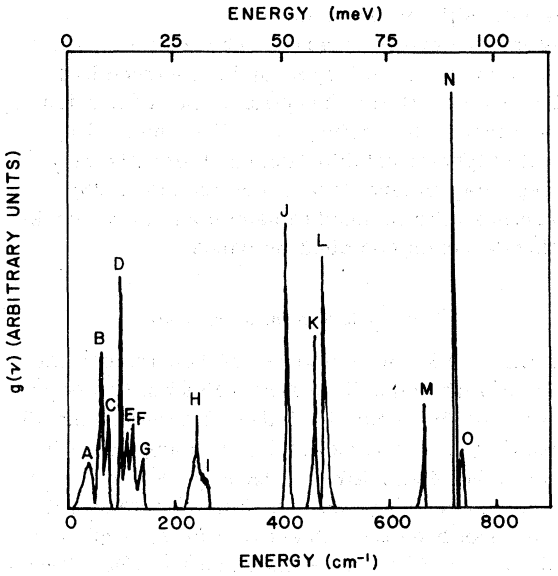


FIG. 7. Calculated phonon density of states for $Cs_2SiF_6$ at 6 K.

time.

The 140-point calculated $g(\omega)$ for $Cs_2SiF_6$ is shown in Fig. 7. The individual peaks in the calculated spectrum have been labeled. We must now identify the origin of each of these peaks. The distribution function $g(\omega)$ can be expressed[12] as a sum over the vibrational mode branches

$$g(\omega) = \sum_{j=1}^{27} g_j(\omega) , \tag{5}$$

with

$$g_j(\omega) = \frac{V}{(2\Pi)^3} \frac{1}{3} \int_{S(\omega)} \frac{dS}{|\vec{\nabla}\omega_j(\vec{q})|} . \tag{6}$$

TABLE IV. Composition of the calculated phonon density of state peaks shown in Fig. 7.[a]

| Peak | Energy ($cm^{-1}$) | Assignment |
|---|---|---|
| *A* | 37 | $TA(L_3^-)$ |
| *B′* | 58 | $LCs^+(X_2^-)$ |
| *B* | 63 | $TCs^+(L_3^+)$ |
| *C* | 75 | $LCs^+(L_1^+)$, $LA(L_2^-)$ |
| *D* | 100 | TO |
| *E* | 111 | $LO(L_2^-)$ |
| *F* | 121 | $Rot(X_5^+)$ |
| *G* | 140 | $LO(\Gamma)$, $Rot(L_2^+)$ |
| *H* | 239 | $T\nu_6$ |
| *I* | 253 | $L\nu_6$ |
| *J* | 405 | $\nu_5$ |
| *K* | 458 | $\nu_2$ |
| *L* | 474 | $L\nu_4$ |
| *M* | 663 | $\nu_1$ |
| *N* | 721 | $T\nu_3$ |
| *O* | 734 | $L\nu_3$ |

[a]Note that 1 meV = 8.066 $cm^{-1}$.

Here $S(\omega)$ is a surface of constant frequency $\omega = \omega_j(\vec{q})$, and $V$ is the volume of the unit cell. In general, $g(\omega)$ will contain a singularity where $\vec{\nabla}\omega_j(\vec{q}) = 0$, and in regions of high symmetry this will often give a large density of phonon states. These singularities are known as critical points or Van Hove singularities.[13] The phonon character of each of the peaks in Fig. 7 has been determined by assuming that they result from the high-symmetry dispersion curves where $\vec{\nabla}\omega_j(\vec{q}) = 0$. The results are given in Table IV.

## V. INTERPRETATION OF VIBRATIONAL AND VIBRONIC SIDEBAND RESULTS

### A. Vibrational Raman analysis

The Raman effect in solids is the inelastic scattering of photons by phonons. In the first-order Raman scattering process the incident photon $(\omega_i, \vec{k}_1)$ is scattered within the solid to create or destroy a phonon $(\omega_j, \vec{q})$, and a photon of frequency and wave vector $(\omega_f, \vec{k}_f)$ is emitted such that conservation of energy and momentum occurs:

$$\omega_i = \omega_f \pm \omega_j , \tag{7}$$

$$\vec{k}_i = \vec{k}_f \pm \vec{q} . \tag{8}$$

Also, there is the symmetry requirement that the phonon transforms according to the proper irreducible representation. In first-order Raman scattering, $|k_i|$ is about $10^5$ $cm^{-1}$, and this is much less than the zone boundary $|\vec{q}|$ crystal value; thus only phonons from the center of the Brillouin zone can be involved.

Standard group theory[14] shows that at the Brillouin zone center, phonons that transform as the $\Gamma^{1+}$, $\Gamma^{3+}$, and $\Gamma^{5+}$ irreducible representations will be Raman active in a pure $Fm3m$ $Cs_2SiF_6$-type crystal. If the 6 K Raman data for $Cs_2SiF_6$ (Fig. 2) are compared with the zone-center vibrational mode Raman-active irreducible representations, we can assign the 68.8-$cm^{-1}$ peak to the cation-motion mode which transforms as $\Gamma^{5+}$. Also, the 401 $cm^{-1}$ peak is assigned to the $\Gamma^{5+}$ internal vibrational bending mode, and the two higher energy peaks at 647 and 469 $cm^{-1}$ are assigned to the $\Gamma^{1+}$ and $\Gamma^{3+}$ internal stretching modes.

Chodos, Black, and Flint[6] (CBF) have reported the Raman spectrum at room temperature for $Cs_2SiF_6$ and $Cs_2GeF_6$. Their results are very similar to the Fig. 3 data with the single exception that a weak peak is observed at 38 $cm^{-1}$ in the room-temperature experiments. CBF suggest that this peak could be due to the $L^{3-}$ zone-boundary acoustic-mode observable via a lattice imperfection, or could be due to a difference band. The lattice-imperfection hypothesis can be tested

by using results of Loudon.[15] He has shown that the presence of a single substitutional or vacancy defect reduces the symmetry group of the system from the crystal space group to the point group of a lattice site. Thus, from the Loudon tables, it follows that the $L^{3-}$ transverse acoustic mode at 34 $cm^{-1}$ reduces in the cubic site symmetry to the $\Gamma^{3-}$, $\Gamma^{4-}$, and $\Gamma^{5-}$ irreducible representations and, because of inversion symmetry, is not Raman active. Thus the peak at 38 $cm^{-1}$ probably arises from a two-phonon process. A possible assignment is LA($X^{4-}$)-TA($X^{5-}$).

### B. Vibrational infrared analysis

For an infrared absorption process, a photon may be absorbed provided the wave vector and energy are conserved. The first-order infrared process consists of only zone-center excitations. Multiphonon-absorption combinations are governed by the relations[16]

$$\omega = \sum_i (\pm \omega_i) , \tag{9}$$

$$\vec{q} + \vec{n}\tau = \sum_i (\pm \vec{k}_i) , \tag{10}$$

where $\omega$ and $\vec{q}$ are the energy and the wave vector of the absorbed photon, $\omega_i$ and $\vec{k}_i$ are the energy and the wave vector of the $i$th photon, $\vec{\tau}$ is a reciprocal-lattice vector, and $n$ is an integer. For one- and two-phonon processes, $n = 0$, and for a three-phonon process, $n = 0, \pm 1$.

We can apply these conservation rules to assign the available infrared data for $Cs_2SiF_6$. The far-infrared spectrum of $Cs_2SiF_6$ at 80 K has been reported by Chodos, Black, and Flint.[6] They observed a strong broad band at 106 $cm^{-1}$ which they assign to the zone-center TO lattice mode and a shoulder at 121–126 $cm^{-1}$. The TO lattice-mode assignment is in satisfactory agreement with the 6 K inelastic neutron scattering result of 98 $cm^{-1}$. For the shoulder at 121–126 $cm^{-1}$, CBF assign this to the longitudinal-optical (LO) mode allowed by lattice imperfections. The neutron results indicate that the zone-center LO energy is about 135 $cm^{-1}$, which rules out the CBF interpretation. An alternative explanation is to assign the observed peak as a multiphonon band.

The infrared spectrum in Fig. 4 can be assigned from a consideration of all the multiphonon combination bands. Here, combination bands of the following types must be considered: internal + lattice, internal + internal, and lattice + lattice. The energies and assignments are given in Table II. Peaks 1, 3, 4, 5, 10, and 21 can be assigned to (internal + lattice) combination bands at $\Gamma$ and $L$ symmetry points. These peaks have appreciable intensity and show increased sharpness as the temperature is lowered. The (internal + internal) combination bands can be assigned to $\Gamma$ point modes with the exception of peak 6, which arises from the $L$ point; also, it is interesting that this type of combination band also shows a strong temperature dependence (see peak 20). There has been no need to assign any of the peaks to three-phonon combination bands.

### C. Vibronic sideband assignments

In this section we demonstrate how the optical spectra of an impurity ion-host system can be understood in terms of a lattice-dynamical model. In particular, we consider the $d^3$ manganese (IV) hexafluoride ion, $MnF_6^{-2}$, doped in a $Cs_2SiF_6$-type lattice. In recent years, the $MnF_6^{-2}$ octahedral system has been the subject of a large number of studies.[1a,6,2] The sharp-lines and detailed vibronic structure for the absorption and emission spectra of the $^4A_{2g} \leftrightarrow {}^2E_g$ transition makes the $Mn^{4+}$ ion in cubic symmetry an ideal system for study.

Loudon[15] has discussed the selection rules for phonon assisted electronic transitions in a face-centered cubic lattice in which an impurity ion is substitutionally placed in the lattice. He has pointed out that observed vibronic peaks in the electronic spectrum of the impurity ion can arise from lattice phonons with the correct symmetry consistent with the initial and final electronic-state symmetries, as well as from localized vibrations of the impurity ion which have no analogue in the perfect crystal. Also, it is expected that when the impurity-ion vibrational energies are close to the host-lattice energies, strong coupling can occur if the irreducible representations of the two motions are the same.

Let us now consider the necessary conditions for the appearance of phonons in impurity-ion electronic spectra. The presence of a substitutional defect in an otherwise perfect crystal removes the translational symmetry of the system and reduces the symmetry group of the system from the crystal space group to the point group of the lattice site. Loudon[15] has provided a table for the reduction of the space group representations of a face-centered cubic lattice. Consider an impurity ion that undergoes a vibronic electric-dipole allowed transition, with $\Gamma_i$ and $\Gamma_f$ the irreducible representations of the initial and final electronic states. Since the electric dipole operator transforms as $\Gamma^{4-}$, the selection rule for participation of a phonon is that one of its site symmetry irreducible representations is contained in the direct product $\Gamma_i \times \Gamma^{4-} \times \Gamma_f$. For the $MnF_6^{-2}$ $^4A_{2g} \leftrightarrow {}^2E_g$ transition, phonons with $\Gamma^{4-}$ and $\Gamma^{5-}$ site symmetry irreduci-

ble representations can appear in the vibronic structure.

If the impurity-ion interaction with the host-lattice vibrations is linear with the phonon normal coordinates, the probability $W$ for a transition of the impurity ion from electronic state $i$ to state $f$, with creation of a phonon $(\vec{q}\Gamma)$, is given at low temperatures by[17]

$$W = (2\pi/\hbar)\,|\langle\chi_i|0|\chi_f\rangle|^2 g(\omega)\delta(E-\hbar\omega-E_f)\,, \qquad (11)$$

with

$$\langle\chi_i|0|\chi_f\rangle = \sum_p \left(\frac{\hbar}{2\omega_{\vec{q}\Gamma}}\right)^{1/2}\left(\frac{\langle\psi_i|f_{\vec{q}\Gamma}|\psi_p\rangle\langle\psi_p|0|\psi_f\rangle}{E_i-(E_p+\hbar\omega_{\vec{q}\Gamma})}+\frac{\langle\psi_i|0|\psi_p\rangle\langle\psi_p|f_{\vec{q}\Gamma}|\psi_f\rangle}{(E_f+\hbar\omega_{\vec{q}\Gamma})-E_p}\right). \qquad (12)$$

0 is the electric dipole operator and $f_{\vec{q}\Gamma}$ is the part of the interaction Hamiltonian $H^1$ ($H^1=\sum_{\vec{q}\Gamma} f_{\vec{q}\Gamma}Q_{\vec{q}\Gamma}$) which operates only on the impurity electronic states. For the initial state, $|\chi_i\rangle$, the phonon state belongs to the identity representation, and thus $|\chi_i\rangle$ transforms the same way as the initial electronic state $|\psi_i\rangle$; also, the final state $|\chi_f\rangle$ involves the electronic state $|\psi_f\rangle$ and a phonon with energy $\hbar\omega_{\vec{q}\Gamma}$. From Eqs. 11 and 12 we expect vibronic transitions to be observed at those phonon energies where the phonon density of states peaks. The relative strength of an individual vibronic transition will be governed by the selection rules for the phonons which contribute to the phonon density of states (PDS) peak and by the magnitude of the $\langle\chi_i|0|\chi_f\rangle$ matrix element. Thus if a particular PDS peak involves phonons with only gerade symmetry, that particular peak will not appear in the experimental $MnF_6^{-2}$ $d$-$d$ vibronic spectrum. In addition, even in a PDS peak arises from phonons with the correct site symmetry, there is the additional requirement from Eq. (12) that these phonons provide a changing crystal field at the metal impurity site location. If this does not occur, then $\langle\chi_i|0|\chi_f\rangle = 0$, and the PDS peak cannot appear in the impurity-ion vibronic spectrum.

Recently Manson *et al.*[2] have measured the detailed ${}^2E_g - {}^4A_{2g}$ emission spectrum at liquid-helium temperatures for $(MnF_6)^{-2}$ impurities in the $Cs_2SiF_6$ system. A summary of the major peaks and relative intensities is given in Table V for the 0–200-$cm^{-1}$ region. In addition, Manson[18] has determined from magnetic circular emission measurements that the excitation at 70 $cm^{-1}$ has predominantly $\Gamma^{4-}$ character. The structure in the luminescence spectrum should be directly due to the host-lattice vibrational spectra. Quantitative comparison of theory and experiment, however, would require detailed calculations of the matrix elements in Eq. (11), which would, in turn, necessitate precise evaluation of the electronic wave functions of the impurity ion. A qualitative understanding can nevertheless be achieved by use of the site symmetry selection rules.

We have used two methods to relate the luminescence spectrum to the phonon density of states. First we have simply assumed that all the calculated PDS peaks can appear in the spectrum without any symmetry restrictions. In this case the assignments have been made by comparing the energies as well as the intensities of the peaks. We note first of all that with all transitions allowed

TABLE V. Summary of $Cs_2MnF_6 - Cs_2SiF_6$ ${}^2E \rightarrow {}^4A_{2g}$ emission data at 15 K and phonon density of state peak assignments.

| Emission experimental results at 15 K [a] | | | $Cs_2SiF_6$ PDS assignment | |
|---|---|---|---|---|
| Peak no. | Vibrational Energy ($cm^{-1}$) | Relative intensity | PDS peak assignment (see Table IV) | Site symmetry of PDS peak from Loudon Tables [b] |
| 1 | 41 | 3.8 | $A$ (37 $cm^{-1}$) | $\Gamma^{3-}+\Gamma^{4-}+\Gamma^{5-}$ |
| 2 | 59 | 5.9 | $B'$ (58) | $\Gamma^{3-}+\Gamma^{4-}$ |
| 3 | 70 | 10.0 | $C$ (75) | $\Gamma^{4-}$ |
| 4 | 104 | 4.5 | $D$ (100) | TO $(\Gamma^{4-})$ [c] |
| 5 | 120–130 | 2.3 | $G$ (140) | $(\Gamma^{4-})$ [c] |
| 6 | 160 | 9.5 | $B+D$ (163) | $\Gamma^{4-}+\Gamma^{5-}$ |
| 7 | 191 | 3.2 | $C+E$ (186) | $\Gamma^{4-}+\Gamma^{5-}$ |

[a] Emission experiments carried out in our laboratory on $MnF_6^{-2}$ in $Cs_2GeF_6$ at 1.8 K show similar phonon structure but peaks 6 and 7 have smaller relative intensities.

[b] If the site symmetry is $\Gamma^{4-}$ or $\Gamma^{5-}$ then the PDS peak, from symmetry considerations, can appear in the ${}^4A_{2g} \leftrightarrow {}^2E_g$ spectrum.

[c] Split into transverse and longitudinal components.

that there are more peaks predicted than observed. In addition, the peak at 70 $cm^{-1}$ might be assigned on the basis of intensity considerations to peak $B$ in Fig. 7, which does not have $\Gamma^{4-}$ symmetry as required by experiment. It is therefore clear that proper account of the site symmetry selection rules and matrix elements must be taken in order to understand the luminescence spectrum.

For the second model to assign the $Mn^{4+}$ luminescence spectrum, we have assumed that the PDS peaks do not appear in the experimental optical spectrum unless site symmetry selection rules are obeyed. Thus, for peaks $A$–$G$ in the PDS calculated spectrum, Loudon's tables have been used to determine if the critical points corresponding to each peak have $\Gamma^{4-}$ or $\Gamma^{5-}$ site symmetry, and thus should appear in the spectrum. PDS peaks $B$, and $F$ are not allowed because they possess gerade inversion site symmetry. The remaining PDS peaks $A$, $B'$, $C$, $D$, and $G$ can be correlated with experimental vibronic spectrum peaks with about the correct energy. Also, peak 3 is now predicted to have only $\Gamma^{4-}$ site symmetry, in agreement with the Manson measurements. Two strong peaks at 160 and 191 $cm^{-1}$ in the optical spectrum do not correspond to single PDS peaks and are thus assigned to two phonon combinations, $L_3^+ + L_3^-$ and $L_2^- + L_1^+$, respectively. These two phonon combination bands possess $\Gamma^{4-}$ or $\Gamma^{5-}$ site symmetry, and thus are in agreement with the Loudon selection rules. In Table V a tabulation of the assignments is presented.

We have demonstrated that the phonon-assisted peaks that appear in the experimental $^2E_g \rightarrow {}^4A_{2g}$ $Cs_2MnF_6$-$Cs_2SiF_6$ optical spectrum for $E < 200$ $cm^{-1}$ can be assigned to specific high-symmetry critical points in the phonon spectrum for $Cs_2SiF_6$. Furthermore, in the $E > 200$ $cm^{-1}$ portion of the experimental optical spectrum, Chodos, Black, and Flint[6] have assigned the 16 multiphonon bands involving four low-frequency lattice modes with energies of about 41, 67, 104, and 127 $cm^{-1}$. These modes can be assigned to PDS peaks $A$, $C$, $D$, and $G$ in Fig. 7.

## VI. SUMMARY

The primary result of this paper is to report phonon dispersion curves for the cubic antifluorite material $Cs_2SiF_6$. It has been shown that the 14-parameter O'Leary and Wheeler rigid-ion model provides a reasonable representation of the lattice dynamics of a $Cs_2MF_6$-type system. Second, the infrared and Raman spectra of $Cs_2SiF_6$ at low temperatures can be assigned in a fairly simple fashion by invoking only single- and double-phonon combination bands of the proper symmetry.

Finally, in an attempt to identify the phonons that participate in phonon-assisted optical $d$-$d$ transitions in mixed-crystal $A_2MX_6$-type systems, we have compared the luminescence spectrum of the $^2E_g \rightarrow {}^4A_{2g}$ transition of Mn(+4) doped in $Cs_2SiF_6$ with the $Cs_2SiF_6$ phonon density of states. We find that the phonon density of states, coupled with the impurity site symmetry relations of Loudon, is sufficient to understand the low-energy structure observed in the luminescence spectrum.

## ACKNOWLEDGMENTS

We wish to express our gratitude to G. Shirane, J. D. Axe, H. Engstrom, M. C. McKeown (Brookhaven), R. G. Wheeler (Yale), P. B. Dorain (Brandeis), S. Bishop (Naval Research Laboratory), S. J. Pickart (University of Rhode Island), and L. Helmholz (Washington University) for their help. Also, we want to thank N. Manson (Australian National University) for informing us of his $Cs_2MnF_6$-$Cs_2SiF_6$ optical results. Research at Brookhaven was supported by the Division of Basic Energy Sciences, Department of Energy, under contract No. EY-76-C-02-0016. H.H.P.'s research at Maine was supported by the NSF Material Science Division, DMR 77-07140.

---

*Guest Scientist at Brookhaven National Laboratory.
†Present address: Dept. of Physics, University of Maryland, College Park, Maryland 20742.

[1]Selected representative papers are: (a) L. Lindsay Helmholtz and M. E. Russo, J. Chem. Phys. 59, 5455 (1973); (b) P. B. Dorain and R. G. Wheeler, J. Chem. Phys. 45, 1142 (1965) and P. B. Dorain, H. H. Patterson, and P. C. Jordan, *ibid.* 49, 3845 (1968); (c) T. A. Keiderling, P. J. Stephens, S. B. Piepho, J. L. Slater, and P. N. Schatz, Chem. Phys. 11, 343 (1975) and J. C. Collingwood, S. B Piepho, R. W. Schwartz, P. A. Dobosh, J. R. Dickinson, and P. N. Schatz, Mol. Phys. 29, 793 (1975); (d) H. H. Patterson, J. L. Nims, and C. M. Valencia, J. Mol. Spectrosc. 42, 567 (1972) and J. A. LoMenzo, S. Strobridge, and H. H. Patterson, *ibid.* 66, 150 (1977).

[2]D. F. Durocher and P. B. Dorain, J. Chem. Phys. 61, 5182 (1974). However, the reader should also see W. C. Yeakel, R. W. Schwartz, H. G. Brittain, J. L. Slater, and P. N. Schatz, Mol. Phys. 32, 1751 (1976), as well as N. B. Manson, G. A. Shah, B. Howes, and C. D. Flint, *ibid.* 34, 1157 (1977).

[3]G. O'Leary and R. G. Wheeler, Phys. Rev. B 1, 4409 (1970).

[4]D. Durocher and P. B. Dorain, J. Chem. Phys. 61, 1361 (1974).

[5]S. L. Chodas and R. A. Satten, J. Chem. Phys. 62, 2411 (1975).
[6]S. L. Chodas, A. M. Black, and C. D. Flint, J. Chem. Phys. 65, 4816 (1976).
[7]J. L. Lynn, H. H. Patterson, G. Shirane, and R. G. Wheeler, Solid State Commun. 27, 862 (1978).
[8]H. Engstrom, Rev. Sci. Instrum. 47, 928 (1976).
[9]M. Debeau and H. Poulet, Spectrochim. Acta 25A, 1553 (1969).
[10]W. Marshall and S. W. Lovesey, *Theory of Thermal Neutron Scattering* (Oxford University, London, 1971).
[11]G. Gilat and L. J. Raubenheimer, Phys. Rev. 144, 390 (1966).
[12]G. Gilat, Methods in Comput. Phys. 15, 317 (1975).
[13]L. V. Hove, Phys. Rev. 89, 1189 (1953).
[14]F. A. Cotton, *Chemical Applications of Group Theory*, 2nd ed. (Wiley-Interscience, New York, 1971).
[15]R. Loudon, Proc. Phys. Soc. 84, 379 (1964).
[16]J. J. Turner and W. E. Reese, Phys. Rev. 127, 126 (1962); S. S. Mitra, J. Chem. Phys. 39, 3031 (1963).
[17]E. Cohen and H. W. Moos, Phys. Rev. 161, 258 (1967).
[18]N. Manson (private communication).